
1 **Visible-Light Photocatalysis Accelerates As(III) Release and**
2 **Oxidation from Arsenic-containing Sludge**

3 Hongbo Lu,^{†, ¶} Xueming Liu,[‡] Feng Liu,[†] Zhengping Hao,^{†, ¶} Jing Zhang,^{†, ¶} Zhang
4 Lin,[‡] Yvonne Barnett,[¥] and Gang Pan ^{†, *}

5 [†] Key Laboratory of Environmental Nano-technology and Health Effect, Research
6 Center for Eco-Environmental Sciences, Chinese Academy of Sciences, Beijing
7 100085, P. R. China

8 [¶] National Engineering Laboratory for VOCs Pollution Control Materials &
9 Technology, University of Chinese Academy of Sciences, Beijing 101408, P.R. China

10 [‡] School of Environment and Energy, South China University of Technology,
11 Guangzhou 510006, P.R. China

12 [¥] School of Science and Technology, Nottingham Trent University, Clifton Campus,
13 NG11 8NS, UK

14 ^{*} Centre of Integrated Water-Energy-Food Studies (*i*WEF), School of Animal, Rural,
15 and Environmental Sciences, Nottingham Trent University, Brackenhurst Campus,
16 NG25 0QF, UK

17
18 **Abbreviations:** arsenic sulfide sludge (ASS)

19 **ABSTRACT:**

20 Arsenic containing sludge, a product of the treatment of acid smelting

21 wastewater, is susceptible to temperature, pH, co-existing salt ions and organic matter,
22 which might lead to the release of arsenic ions into the environment. Here, we studied
23 the effect of visible light on the dissolution and oxidation of arsenic sulfide sludge
24 (ASS) sampled from a smelting plant. Results show that by exposure to visible light,
25 both the release of As(III) ions from ASS and the oxidation of As(III) into As(V) were
26 markedly accelerated. Electron paramagnetic resonance (EPR) and free radical
27 quenching experiments revealed that ASS acts as a semiconductor photocatalyst to
28 produce hydroxide and superoxide free radicals under visible light. At pH 7 and 11,
29 both the dissolution and the oxidation of the sludge are directly accelerated by $\cdot\text{O}_2^-$.
30 At pH 3, the dissolution of the sludge is promoted by both $\cdot\text{O}_2^-$ and $\cdot\text{OH}$, while the
31 oxidation of As(III) is mainly controlled by $\cdot\text{OH}$. In addition, the solid phase of ASS
32 was transformed to sulfur (S_8) which favored the aggregation and precipitation of the
33 sludge. The transformation was affected by the generation of intermediate sulfur
34 species and sulfur-containing free radicals, as determined by ion chromatography and
35 low-temperature EPR, respectively. A photocatalytic oxidation-based model is
36 proposed to underpin the As(III) release and oxidation behavior of ASS under visible
37 light conditions. This study helps to predict the fate of ASS deposited in the
38 environment in a range of natural and engineered settings.

39 **Keywords:** Arsenic sulfide sludge; photocatalysis, Release; Oxidation; Active free
40 radicals

41 **1. Introduction**

42 Arsenic is ubiquitous in the Earth's crust, with a mean concentration of 0.5–2.5
43 mg/kg – about 0.00005% of the Earth's crust [1]. It often coexists with the ores
44 containing precious and non-ferrous metals, or iron [2]. During metal smelting,
45 mineral processing, and sulfuric acid production from pyrite ores, a large amount of
46 arsenic-containing acid wastewater and tailings are produced [3]. For example, the
47 arsenic concentration in the wastewater from a sulfuric acid plant can range from
48 several to tens of thousands mg/L [4]. One of the most popular techniques for
49 treatment of the arsenic wastewater in industry is sulfide precipitation, where sulfide
50 is employed to transform arsenic ions into arsenic sulfide precipitate [5]. This
51 technique has many advantages, such as low solubility of arsenic sulfide at a low pH,
52 high sediment rate and efficiency, less sludge volume and water content [6,7]. As a
53 result, large quantities of arsenic sulfide slag is discharged into the environment. For
54 example, more than half a million tons of arsenic sludge are produced annually in
55 China.

56 Arsenic sulfide sludge deposited in the environment is susceptible to temperature,
57 pH, coexisting organics and inorganics (e.g. sulfides) [8,9]. The weathered and
58 dissolved residues promote the release of arsenic ions into the surroundings, which
59 can result in the transport and transformation of chemical species (e.g. arsenic and
60 sulfur) in natural waters and so leading to environmental contamination. Previous

61 studies have demonstrated that when pH is higher than 9, the dissolution of artificial
62 As₂S₃ particles is significantly enhanced, owing to the enhanced activity of the
63 hydroxylated surface species [10]. On the other hand, different types of sulfur species
64 can influence the dissolution rate of arsenic sulfide. For instance, the added sulfide
65 ions can react with arsenic sulfide and produce arsenic-sulfide complex (H₂As₂S₆⁻),
66 according to eq 1, which will accelerate the dissolution of the solid [11,12].



68 Recently, the effect of light on the dissolution of minerals containing heavy
69 metals has been studied to elucidate the mechanism of photocorrosion reactions on the
70 release of metal ions, such as antimony and vanadium, from their parental minerals or
71 the synthesized substitutes (e.g. senarmonite (Sb₂O₃) [13], stibnite (Sb₂S₃) [14], and
72 vanadium titano-magnetite [15]). It has been demonstrated that simulated sunlight or
73 UV irradiation can promote the dissolution of minerals and thus release heavy metal
74 ions. Up to this time, no work has been reported on the effect of light-induced
75 photochemical reactions on the fate of actual arsenic sludge from industry. As sunlight
76 is one of the most important climate factors for ecosystems, it inevitably affects the
77 fate of heavy metal slag deposited in the environment. On the other hand, arsenic
78 sulfide is a semiconductor with a band gap (~2.34 eV) in the range of visible light
79 spectrum. It has been reported that photocorrosion of artificial As₂S₃ colloids could
80 occur by light irradiation [16]. Therefore, it is expected that the actual sludge, which

81 mainly contains arsenic sulfide, is photo-responsive under visible light conditions.

82 The objective of the investigations described in this paper was to study the
83 dissolution and transformation mechanisms of actual arsenic-containing sludge under
84 visible light conditions. The release and oxidation kinetics of arsenic and sulfur from
85 the sludge, as well as the structure and state of the solid phase, were examined at
86 different pHs under visible light. The intermediate sulfur species arising during the
87 photoreactions were quantified by ion chromatography. The photo-generated active
88 oxygen and sulfur species were identified by EPR and free radical quenching
89 experiments, and their specific contributions to the transformation of the sludge are
90 discussed. The findings of the present investigation assist in the understanding of the
91 fate and transforming process of arsenic sulfide sludge in the environment.

92

93 **2. Materials and methods**

94 **2.1. Chemicals and materials**

95 The details of all reagents used are provided in the Supporting Information. The
96 arsenic sulfide sludge, a product of acid wastewater treatment, was sampled from a
97 smelting plant in Fujian province, China.

98 **2.2. Photo Reaction System**

99 All the photo reactions were performed in a 250 mL beaker by mixing 0.15 g of
100 the solid sludge with 225 g of H₂O. The concentration of ASS was fixed at 0.67 g/L.

101 The initial pH of the suspension was adjusted with HCl or NaOH solution. A 500-W
102 Xe arc lamp (Shanghai Jiguang Special Lighting Appliance Factory, China) was used
103 as a light source equipped with UV cut filters ($\lambda > 420$ nm). The temperature for all
104 the reactions was room temperature (RT ~ 25 °C) using a water-cooling system. At the
105 appropriate time interval, the liquid samples were taken out and filtered through a
106 0.25 μm filter for further analysis. The dissolved oxygen level was controlled by using
107 a gas-purging tube to inject N_2 or O_2 in the system. In order to study the effects of
108 active species, specific radical scavengers were individually added into the reactor,
109 including 0.1 M tert-butyl alcohol (TBA) for scavenging $\cdot\text{OH}$, 0.1 M methanol
110 (MeOH) for $\text{SO}_4^{\cdot-}$, and 1 mM p-benzoquinone (p-BQ) for $\cdot\text{O}_2^-$.

111 **2.3. Analytical Methods**

112 **2.3.1. Arsenic and sulfur species in the liquid phase**

113 The concentration of As(V) was determined using the colorimetric molybdene
114 blue method, and the total As ions (TAs) were measured after As(III) was oxidized
115 completely by KMnO_4 [17]. S(II) species, including H_2S , HS^- , and S^{2-} , were analyzed
116 using the methylene blue method [18]. The concentration of total sulfur (TS) was
117 measured on an ICP-OES (OPTIMA 8300, PerkinElmer, USA). The quantification of
118 sulfur intermediates, including sulfate (SO_4^{2-}), thiosulfate ($\text{S}_2\text{O}_3^{2-}$), and sulfite (SO_3^{2-}),
119 was determined using an ion chromatograph (IS-2000) equipped with a Dionex
120 IonPacTM AS19 (250 \times 4 mm) column. The details of instrumental setups were

121 described in the SI (Table S1).

122 **2.3.2. Solid phase of the sludge**

123 High-resolution field emission transmission electron microscopy (HRTEM)
124 (JEM-2100F, Japan) and scanning electron microscopy (SEM) (SU8020, Japan) were
125 used to characterize the surface morphology of the solids. X-ray diffraction (XRD)
126 (PANalytical B.V.X'Pert3 Powder) featuring a Cu-K (alpha) source was used to
127 determine the crystal phases of samples. X-ray photoelectron spectroscopy (XPS) was
128 performed on an ESCALAB 250Xi instrument (Thermo Fisher Scientific). The As 3d
129 and S 2p XPS spectra were fitted by the XPSPEAK41 software. A UV-2600
130 spectrometer was used to determine the UV-vis absorption spectra of arsenic sludge.
131 X-ray fluorescence (XRF) was performed on an Axios instrument PW4400
132 (PANalytical B.V.).

133 **2.3.3. EPR analysis of active free radicals**

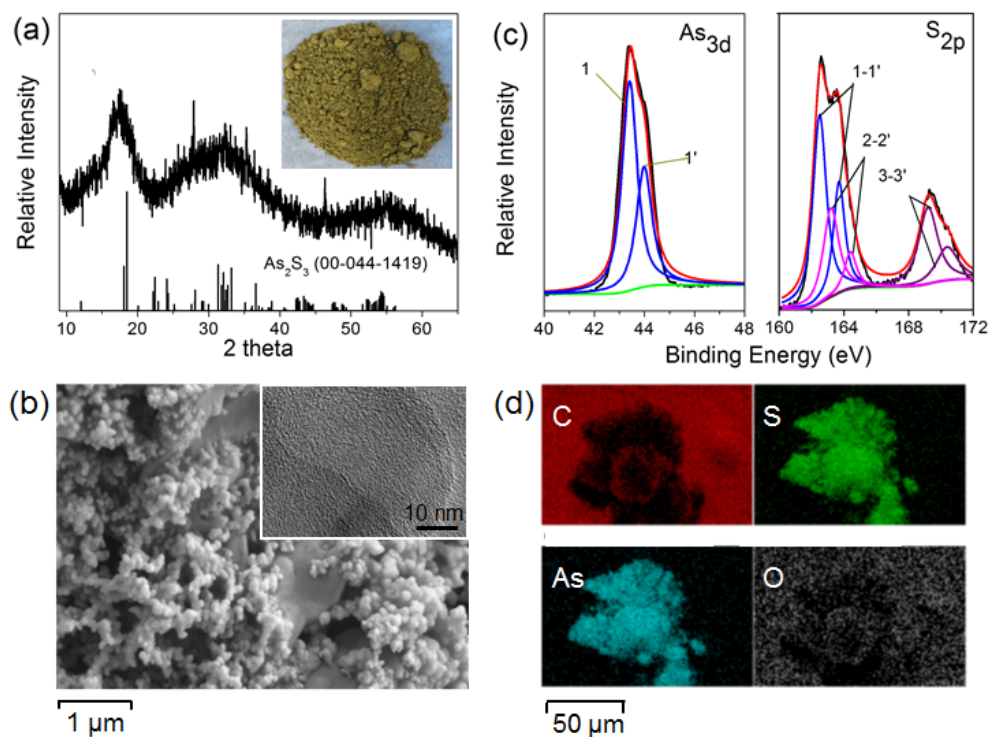
134 $\cdot\text{O}_2^-$, $\cdot\text{OH}$ and SO_3^- radicals were detected on a Bruker EleXsys EPR
135 spectrometer (A300-10/12, Germany) at RT with DMPO as the spin-trapping agent
136 under visible light. When detecting $\cdot\text{O}_2^-$, the methanol was chosen as the dispersion.
137 The sulfur-containing radicals were detected on a Bruker EleXsys EPR spectrometer
138 (E500, Germany) at the low temperature (90 K) using a 100 W mercury lamp
139 equipped with UV cut filters ($2000\text{ nm} > \lambda > 420\text{ nm}$) [19].

140

141 **3. Results and discussion**

142 **3.1. Analysis of raw ASS**

143 The XRD pattern of ASS revealed that the sludge mainly contained nanosized
144 and amorphous As_2S_3 particles plus some undefined impurities (Fig. 1a). The SEM
145 image in Fig. 1b also shows that the sludge comprised of small particles with the
146 size less than 100 nm. HRTEM image (Fig. 1b and Fig. S1) further confirmed that the
147 particles are amorphous structure. EDS mapping images revealed that the two
148 components, As and S, overlapped each other (Fig. 1d). The XRF and ICP-OES
149 results (Table S2) confirm that As and S accounted for the two main components of
150 ASS (more than 80% in mass), while other elements, such as Na, Ni, and Cu,
151 accounted for only 4.18% of the total.

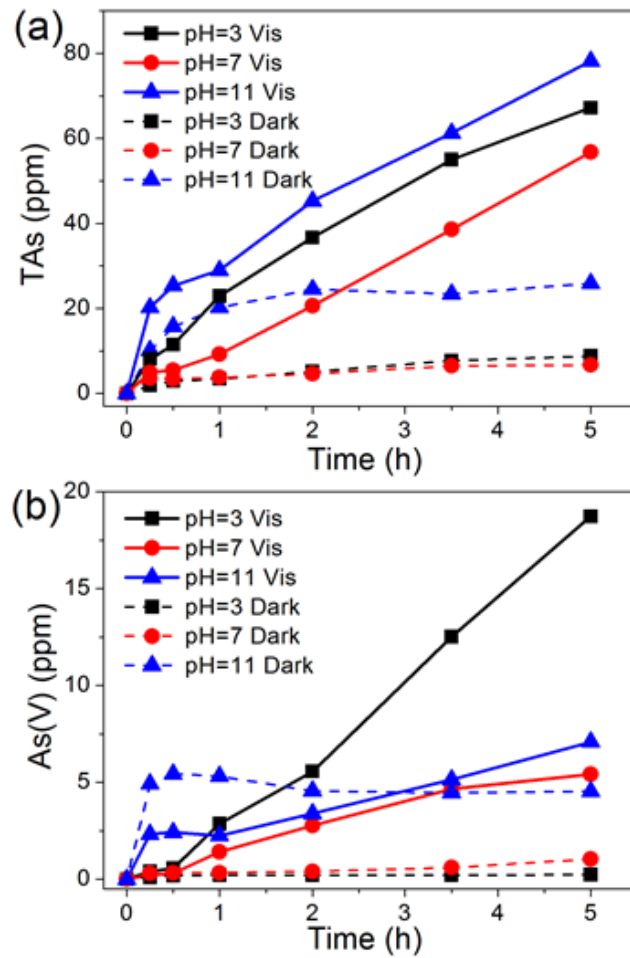


152

153 **Fig. 1.** (a) XRD pattern, (b) SEM image with the inserted HRTEM image, (c) XPS

154 spectra, and (d) EDS mapping images of the raw sludge. In the As 3d spectra, 1 and 1'
155 are assigned to As 3d_{5/2} and As 3d_{3/2}, respectively. In the S 2p spectra, 1, 2, 3 are
156 assigned to S 2p_{3/2}, and 1', 2', 3' are from S 2p_{1/2} of S²⁻ (1-1'), S₂²⁻ (2-2') and SO₄²⁻
157 (3-3'). Inset of (a): optical image of the sludge.

158 XPS spectra (Fig. 1c) of ASS show that the peaks observed ranging from 41 to
159 47 eV, identified as two separated peaks at 43.40 and 44.10 eV (the intensity ratio 5:3),
160 which are ascribed to As 3d_{5/2} and As 3d_{3/2} of As(III), respectively [20]. No As(V) was
161 detected in the system. The peaks from 161 to 170 eV are corresponding to S 2p,
162 which can be fitted by three groups of peaks [21-23]. Each group with a separation of
163 1.2 eV and the intensity ratio of 2:1, is assigned to S 2p_{3/2} and S 2p_{1/2}. The first group
164 of peaks (1-1' in Fig. 1c) located at 162.5 and 163.7 eV originate from S²⁻, while the
165 second pairs (2-2' in Fig. 1c) at 163.2 and 164.4 eV are from S₂²⁻. The third group of
166 peaks at 169.0 and 170.2 eV correspond to SO₄²⁻, indicating that sulfur ions in the
167 sludge were partially oxidized [24].



168

169 **Fig. 2.** Dissolution and oxidation of the sludge in water at different pHs under visible
 170 light irradiation (vis): (a) the release rate of total As (TAs) and (b) the oxidation rate
 171 of As(III).

172

173 3.2. Arsenic release from ASS under visible light

174 The total dissolved arsenic concentration, as a function of time for ASS in
 175 aqueous solution at different pH values, is shown in Fig. 2a. Without light irradiation,
 176 the total arsenic ions (TAs) in solution at pH 3 and pH 7 had a low concentration,
 177 increasing slightly with time. Approximately 8 ppm of TAs could be detected after 5 h

178 at both pH values. At pH 11, TAs in the solution quickly increased with time and
179 reached a plateau after 1 h, where the TAs concentration was about 3 times of that at
180 the low pH. These kinetic observations share similar trends with the results of ref 14,
181 in which the solubility of artificial As_2S_3 particles was independent of pH before pH 6,
182 after which the concentration of TAs increased with pH (as expressed by eq 1).

183 Under visible light irradiation, the dissolution rate of the sludge markedly
184 increased at all the three pH values, as compared to the corresponding cases in the
185 dark. At each pH, the concentration of TAs increased with time, which showed a
186 linear increase after 10 min. On the basis of linear fit (Fig. S2), the dissolution rates of
187 ASS at pH 3, 7 and 11 were 12.61, 11.18, and 12.14 ppm/h, respectively. These data
188 indicated that the illumination by visible light ($\lambda > 420$ nm) can greatly promote the
189 release of arsenic ions from ASS. Moreover, the increase of TAs concentration by
190 light was more pronounced at lower pH. Specifically, the TAs concentration after light
191 irradiation for 5 h was about 8.2, 6.9, and 3.1 times higher, compared to the
192 dissolution in the dark, from low to high pH. These results imply that the
193 light-promoted dissolution of ASS is controlled by the different mechanisms at varied
194 pH values (see the discussion in the section 3.7).

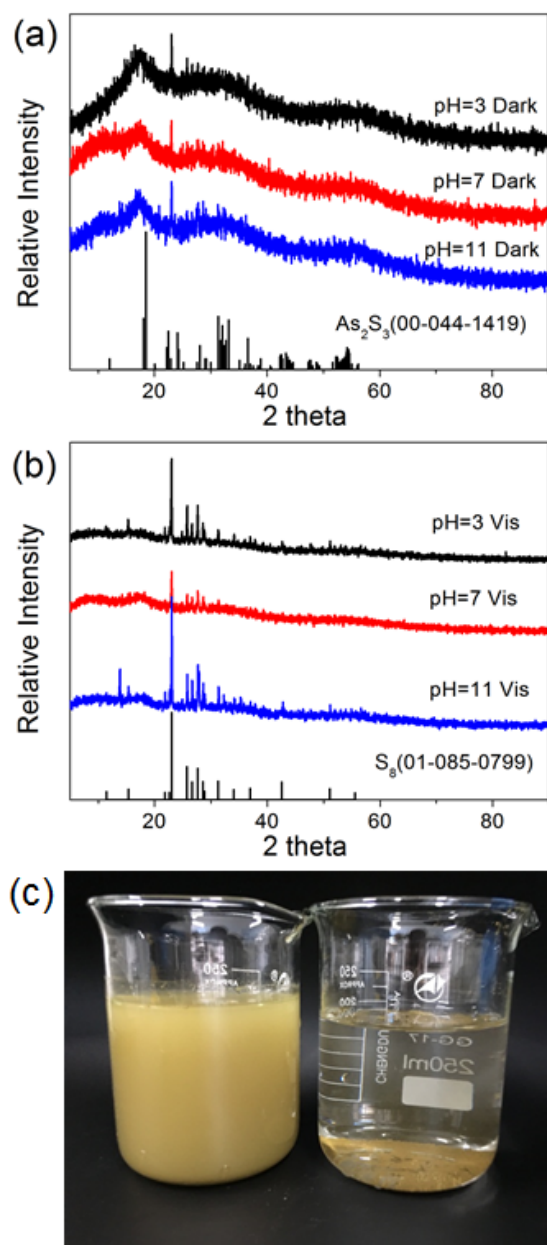
195 **3.3. Arsenic oxidation of ASS under visible light**

196 The concentration of As(V) ions were also measured to check the oxidation of
197 ASS under visible light irradiation. As shown in Fig. 2b, in the dark, almost no As(V)

198 at pH 3 and pH 7, while at pH 11, the concentration of As(V) quickly increased to 4.5
199 ppm at 30 min and then remained at equilibrium. These findings indicated that the
200 oxidation of As(III) into As(V) by oxygen was favored in a basic solution, probably
201 due to the lower redox potential of As(III)/As(V) at higher pH [25].

202 Under visible light, the concentration of As(V) at pH 3 and pH 7 increased with
203 time in a roughly linear mode. Moreover, the oxidation rate of As(III) at pH 3 was
204 much faster than the rate at pH 7 and pH 11. After 5 h of irradiation, the concentration
205 of As(V) at pH 3 was 79.8 times higher than that in the dark, as compared to 5.2 and
206 1.2 times at pH 7 and pH 11, respectively. By linear fit (Fig. S2), the oxidation rates
207 of ASS at pH 3, 7 and 11 were 3.92, 1.16, and 1.02 ppm/h, respectively. These data
208 suggest that the oxidation of As(III) into As(V) is accelerated by light illumination,
209 and more so under acid conditions (see the discussion in the section 3.8). It was
210 notable that at pH 11, a lower concentration of As(V) was obtained at the beginning
211 under visible light than that in the dark. This is probably due to the decrease of pH
212 during the rapid dissolution of ASS under illumination (Table S3), which could
213 change the redox potential of As(III)/As(V) [25]. But with time, the oxidation of
214 As(III) by light was the dominant factor.

215 In addition, the effects of the ASS concentration on the dissolution and oxidation
216 efficiency were checked (Fig. S3). The results indicated that the dissolution and
217 oxidation efficiency of ASS was proportional to the amount of the sludge.



218

219 **Fig. 3.** XRD patterns of the sludge (a) in the dark and (b) under visible light after 5 h.

220 (c) Photo of the sludge in water without light irradiation and sitting for two days (left) ,

221 and under 5 h of visible light irradiation and standing for 2 min (right).

222 3.4. Solid state of ASS after illumination

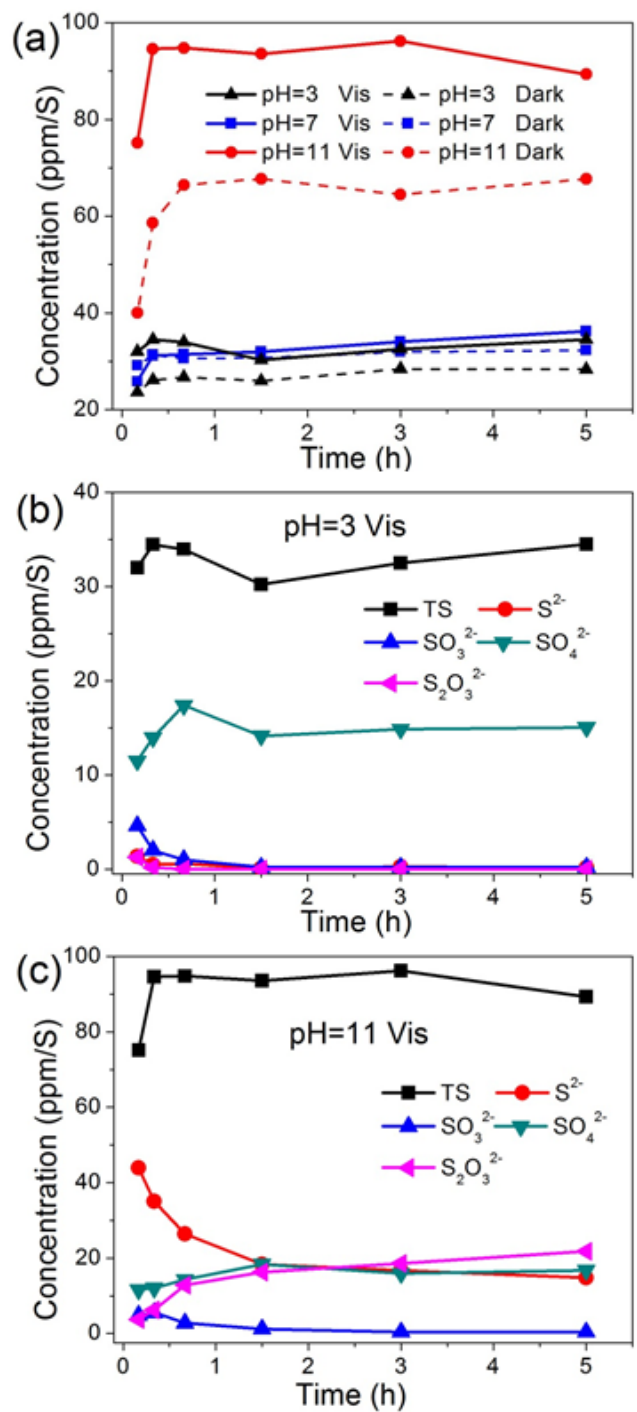
223 Fig. 3a shows that the XRD patterns of ASS remained almost the same under the

224 different pH conditions when in the dark and still kept the characteristic peaks of

225 As_2S_3 . However, an obvious change could be observed after illumination, where the
226 broad peaks from As_2S_3 were suppressed and new sharp peaks occurred (Fig. 3b). The
227 new phase could be identified as S_8 (JCPDS NO.00-044-1419). The species in the
228 ASS with and without visible light irradiation were further characterized by XPS. As
229 shown in Fig. S4, two group of peaks (1-1' and 2-2') located at the binding energies
230 of 162.4-163.6 eV (1-1') and 163.2-164.4 eV (2-2') are corresponding to S 2p of S^{2-}
231 and S_2^{2-} , respectively. But after light irradiation, the ratio of two group peaks for all
232 pH values decreased, indicating that new S species were produced. By fitting the
233 spectra, the peaks can be deconvoluted into two new additional peaks at 163.9 and
234 165.1 eV (3-3'), which are assigned to S $2p_{1/2}$ and S $2p_{3/2}$ of S^0 , respectively [21-23].
235 The XPS results confirm the production of S_8 , which is coincident with the XRD data.
236 From the XPS fitting results (Table S4), the contents of S_8 in the total S after light
237 irradiation were obtained as 14.1%, 10.2%, and 15.2%, at pH 3, 7, and 11,
238 respectively. These data revealed the same pH-dependent order as the dissolution of
239 total arsenic from ASS under illumination, which suggests that the release of arsenic
240 ions from the sludge is accompanied with the generation of S_8 .

241 The precipitation state of ASS in aqueous solution after visible light irradiation
242 was checked and compared with the case without illumination. As shown in Fig. 3c,
243 after 5 h of irradiation the sludge quickly settled down within 2 min and a clear
244 supernatant solution was obtained. Without light irradiation the particles were highly

245 suspended in the solution and complete precipitation could only be achieved after
246 sitting for two days. A great improvement in the sedimentation performance can be
247 reasonably ascribed to both an increase of the particle size and the change of particle
248 surface properties, where the hydrophobic S₈ produced on the surface of the sludge
249 promotes particle aggregation and sedimentation [26].



250

251 **Fig. 4.** (a) Release rate of total sulfur (TS) under visible light irradiation at different

252 pHs. (b and c) Release rate of different sulfur species (TS, S^{2-} , SO_3^{2-} , SO_4^{2-} , and

253 $S_2O_3^{2-}$) at pH 3 (b) and pH 11 (c).

254

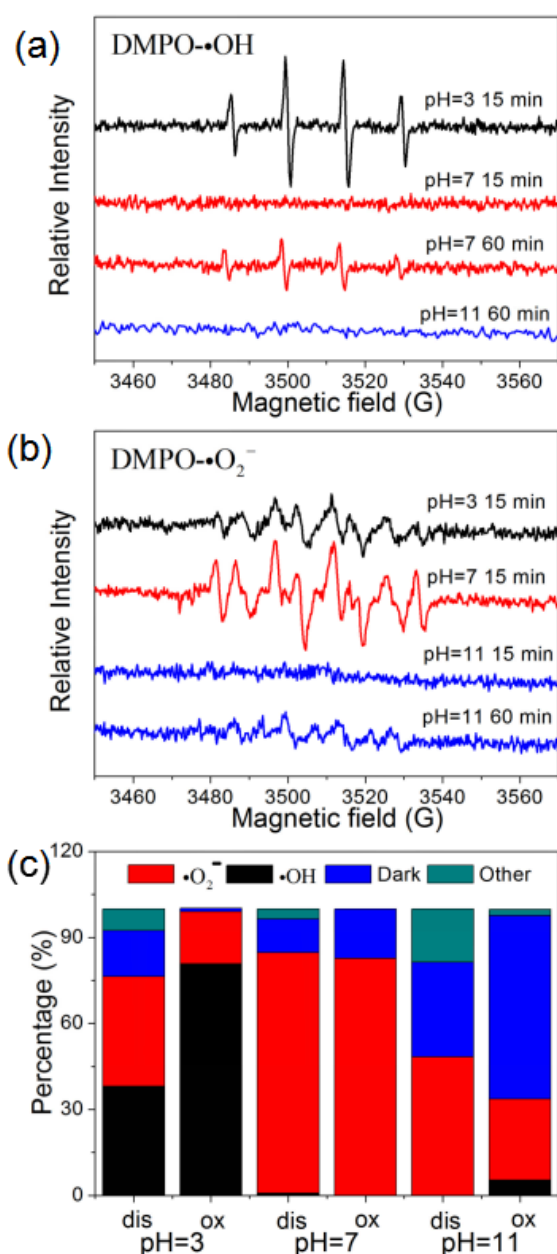
255 3.5. Sulfur speciation released in the solution

256 As mentioned above, not only the release and oxidation of As from ASS, but also
257 the phase transformation from As_2S_3 to S_8 , are accelerated under visible light
258 irradiation. To get a better understanding of the transition of sulfur during the
259 dissolution of ASS, the sulfur species in the system were monitored.

260 Fig. 4a shows that the concentration of Total Sulphur (TS) in the solution
261 increased with pH increasing without light irradiation, where a distinctive increase
262 can be seen at pH 11. These data demonstrated similar trends with the pH-dependent
263 release of arsenic in solution. Under visible light illumination the release of TS was
264 accelerated at all pH values. However, there was only a limited increase of TS at pH 3
265 and 7, while at pH 11, a distinct increase of about 25 ppm/S was observed after 2 h of
266 light illumination, as compared to that in the dark.

267 Specifically, the sulfur species, including SO_4^{2-} , S^{2-} , SO_3^{2-} and $\text{S}_2\text{O}_3^{2-}$, were
268 detected under visible light (Fig. 4b and 4c). At pH 3, SO_4^{2-} increased quickly with
269 time and dominated in solution, accounting for about 50% (15.6 ppm/S) of TS at
270 equilibrium. The reduced and intermediate sulfur species, such as S^{2-} and SO_3^{2-} and
271 $\text{S}_2\text{O}_3^{2-}$, decreased to a very low concentration with time. These data suggest that sulfur
272 might be first dissolved in the form of reduced sulfur species and finally oxidized into
273 SO_4^{2-} . It is worth noting that the concentration of TS was higher than the sum of all
274 the detected S species, probably due to the reason that other sulfur species, such as

275 polythionates ($S_nO_6^{2-}$, $n = 3, 4, 5$ or 6) [27], were not able to be separated or detected.
276 At pH 11, SO_4^{2-} , S^{2-} and $S_2O_3^{2-}$ had an equivalent concentration (~ 20 ppm/S) and
277 these three species mainly contributed to the TS. Comparing to sulfur species at pH 3,
278 a higher concentration of S^{2-} and $S_2O_3^{2-}$, can be found at pH 11. This indicates that the
279 sulfur oxidation under light irradiation in the basic solution is less favorable than that
280 in the acid condition, which is consistent with the arsenic oxidation at different pH
281 values.



282

283 **Fig. 5.** EPR spectra of (a) DMPO-·OH and (b) DMPO-·O₂⁻ produced by light

284 irradiation at different pH (Measurement conditions: 25 mM DMPO and RT), and (c)

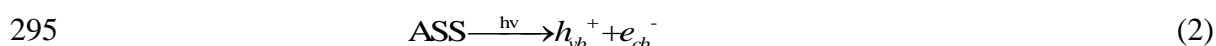
285 Contribution ratio of dissolution (dis) and oxidation (ox) of the sludge by ·OH and

286 ·O₂⁻ after 5 h of light irradiation at different pH (calculated from the concentration of

287 TAs and As(V)).

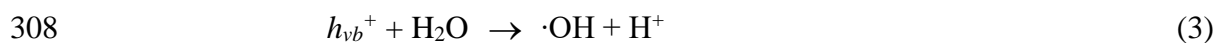
288 3.6. Evaluation of photo-generated active oxygen species

289 It is known that As_2S_3 is a semiconductor with a band gap of 2.34 eV. In the ASS
290 investigated, the measured band gap was 1.89 eV (Fig. S5), indicating a strong
291 absorption and photocatalytic activity in visible light region. Therefore, under visible
292 light irradiation the ASS could generate photo-generated holes (h_{vb}^+) and electrons
293 (e_{cb}^-) (eq 2), which will further react with the species, such as oxygen, hydroxide, and
294 sulfur, to produce active free radicals.

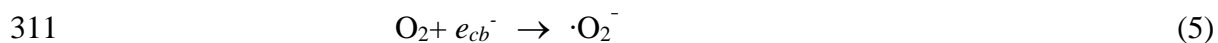


296 EPR was used to directly evidence the generation of the involved free radicals in
297 ASS under visible light irradiation. As shown in Fig. 5a, at pH 3, a strong DMPO- $\cdot\text{OH}$
298 [28] signal could be clearly observed by illumination for 15 min. At pH 7, only a
299 weak DMPO- $\cdot\text{OH}$ signal appeared even after illumination for 1 h. But at pH 11, no
300 signal of hydroxyl radical was detected. These data indicate that the concentration
301 of $\cdot\text{OH}$ decreased with the increase of pH values. Meanwhile, the superoxide radical
302 was also monitored and as shown in Fig. 5b, the characteristic peaks of the
303 DMPO- $\cdot\text{O}_2^-$ [29,30] were detected at all three pH values, although the intensities from
304 $\cdot\text{O}_2^-$ at pH 3 and pH 7 were stronger than that at pH 11. Notably, in the dark, neither
305 $\cdot\text{O}_2^-$ nor $\cdot\text{OH}$ was detected in the all corresponding systems (Fig. S6).

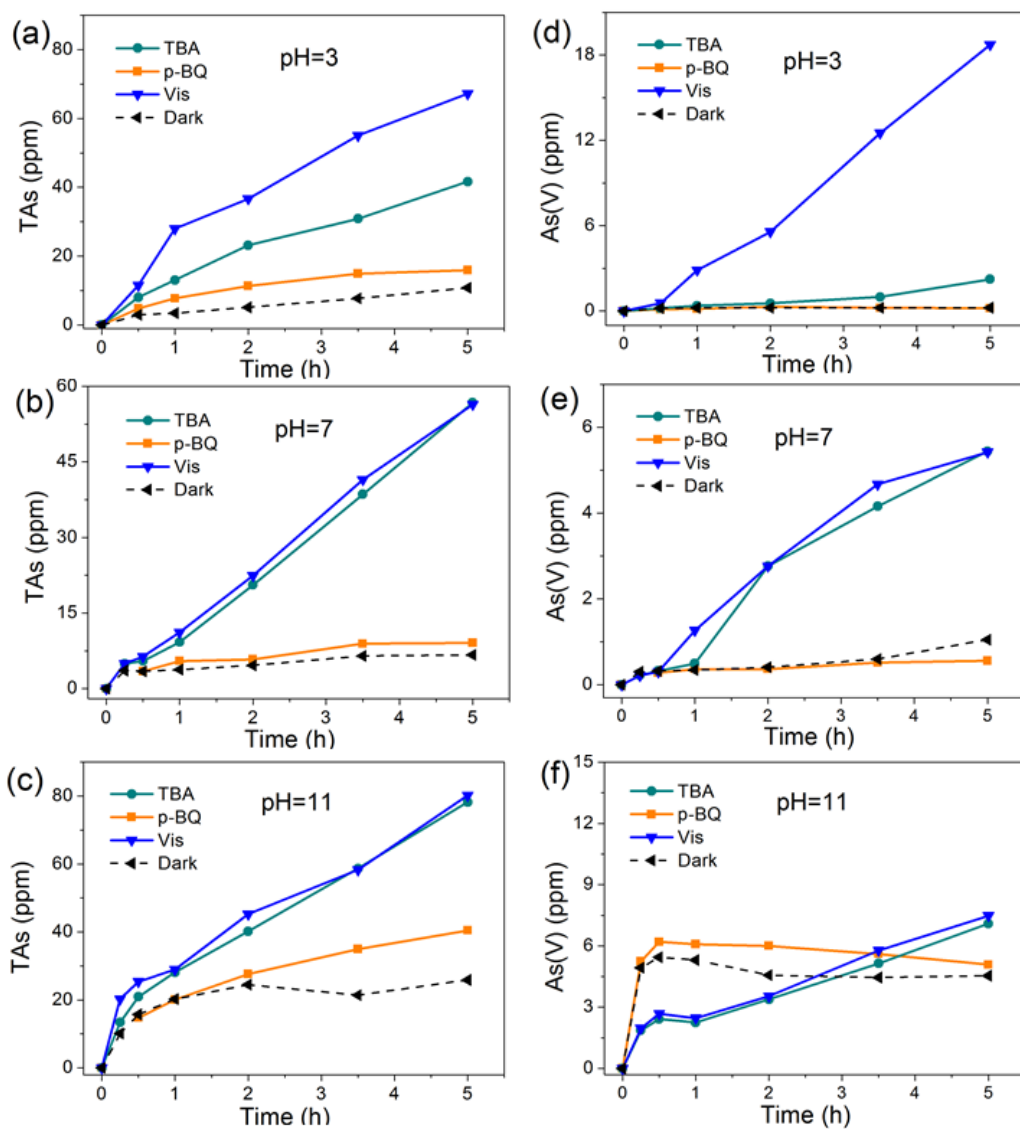
306 On the basis of photocatalytic mechanism, normally $\cdot\text{OH}$ can be produced in two
307 ways, one of which is directly generated from h_{vb}^+ : [31,32]



310 The other way is from e_{cb}^- in the presence of O_2 via a multistep reaction: [33,34]



316 It can be seen from the above reactions that $\cdot\text{OH}$ generated from h_{vb}^+ is more
317 favorable in a neutral or basic condition, while a low pH and dissolving oxygen help
318 to produce $\cdot\text{OH}$ from e_{cb}^- . From our EPR results that show a higher concentration of
319 $\cdot\text{OH}$ obtained at the low pH, it can be deduced that $\cdot\text{OH}$ in the system is probably
320 generated via $\cdot\text{O}_2^-$ in the multistep reaction shown above.



321

322 **Fig. 6.** Quenching effects of the radical scavengers, TBA and p-BQ, on the dissolution
 323 (a-c) and oxidation (d-f) of the sludge at different pHs.

324

325 3.7. The effects of $\cdot\text{O}_2^-$ and $\cdot\text{OH}$ on arsenic release

326 In order to study the effect of different free radicals on the dissolution and
 327 oxidation of ASS, TBA and p-BQ were used as the scavengers to quench $\cdot\text{OH}$ and
 328 $\cdot\text{O}_2^-$, respectively [35,36]. As shown in Fig. 6a-c, in the presence of p-BQ ($\cdot\text{O}_2^-$

329 quencher), the release of TAs from ASS was effectively suppressed at all three pH
330 values. When TBA ($\cdot\text{OH}$ quencher) was added, TAs release was partially inhibited at
331 pH 3 (~33% cut), and with pH increasing, the inhibitory effect was decreased and
332 hardly observed at pH 11. The results revealed that both $\cdot\text{OH}$ and $\cdot\text{O}_2^-$ contributed to
333 the release of TAs at pH 3, but only $\cdot\text{O}_2^-$ contributed at the high pH 7 and pH 11.
334 Their contributions are summarized in Fig. 5c.

335 As discussed above (eq 5-9), $\cdot\text{OH}$ was generated from $\cdot\text{O}_2^-$ in the system, which
336 means that the dissolution of arsenic from the sludge basically originates from the
337 contribution of $\cdot\text{O}_2^-$. So when p-BQ was added in the system at pH 3, most of the
338 dissolution of TAs was suppressed, because the scavenger can both directly inhibit
339 $\cdot\text{O}_2^-$ and indirectly eliminate $\cdot\text{OH}$ that originally stemmed from $\cdot\text{O}_2^-$.

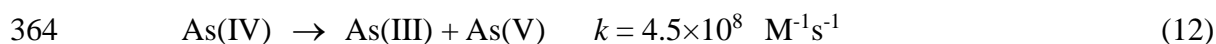
340 The effects of reactive oxygen species on accelerating the dissolution of ASS
341 were further proved by purging O_2 or N_2 in the systems (Fig. S7). The released TAs
342 were obviously increased by purging O_2 at all three pH values, while suppressed by
343 purging N_2 in the solution, although a simply purging N_2 failed to achieve an anoxic
344 condition through completely excluding the dissolved oxygen.

345 **3.8. The effects of $\cdot\text{O}_2^-$ and $\cdot\text{OH}$ on arsenic oxidation**

346 As shown in Fig. 6d-f, the effects of $\cdot\text{O}_2^-$ and $\cdot\text{OH}$ on the oxidation of As(III) into
347 As(V) shared similar trends with the release of arsenic from the sludge (Fig. 6a-c). At
348 pH 3, both TBA and p-BQ reduced the concentration of As(V) close to zero,

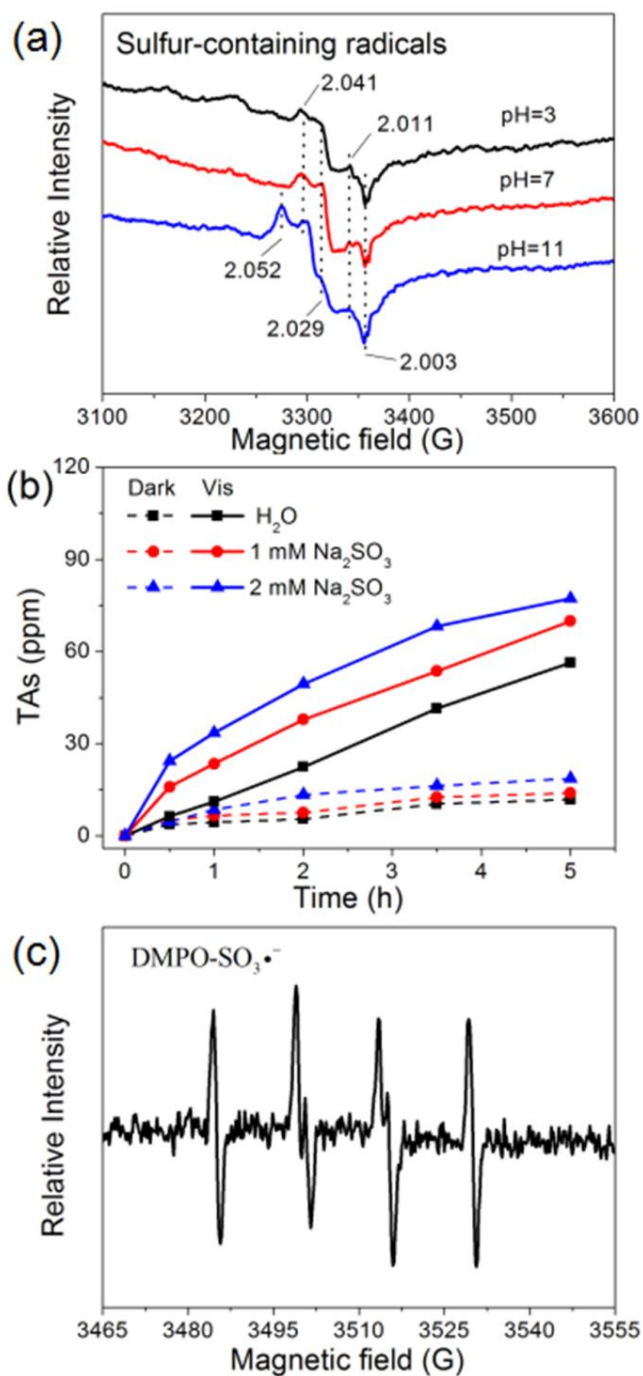
349 suggesting that the oxidation of the released As(III) is effectively suppressed. At the
350 high pH values (7 and 11), TBA had little impact on the concentration of As(V), but
351 p-BQ suppressed almost all the production of As(V). The contributions of different
352 radicals to the oxidation of As(III) is summarized in Fig. 5c. It demonstrates that both
353 $\cdot\text{OH}$ and $\cdot\text{O}_2^-$ can oxidize As(III) into As(V). But at the low pH, $\cdot\text{OH}$ contributed more
354 to the oxidation of As(III). As $\cdot\text{OH}$ has a higher oxidation potential than $\cdot\text{O}_2^-$, more
355 As(V) was thus obtained at pH 3 (Fig. 2b), even if the concentration of total arsenic
356 ions released in the solution was less than that at pH 11 (Fig. 2a). As discussed before,
357 TBA directly scavenges $\cdot\text{OH}$, while p-BQ consumes $\cdot\text{O}_2^-$ and thus indirectly inhibits
358 the generation of $\cdot\text{OH}$. Our results reveal that $\cdot\text{O}_2^-$ is the critical radical in the system
359 and controls the oxidation of As(III).

360 The pathway of As(III) being oxidized into As(V) is proposed as follows (eqs
361 10-13):[37,38]



366 During the oxidation process, As(IV) is the intermediated arsenic species, which will
367 finally transform to As(V) via a As(IV) disproportionation reaction (eq 12) or by
368 further oxidizing with the dissolved O_2 (eq 13) [38]. From eq 10 and 11, it can be seen

369 that the oxidation rate of As(III) by $\cdot\text{OH}$ is much higher than $\cdot\text{O}_2^-$. So, the
370 concentration of As(V) at pH 7 and 11 is obviously smaller than that at pH 3.
371 However, the oxidation-reduction potential of As(V)/As(III) also decreases with the
372 increase of pH values [25]. For example, $E^\circ(\text{As(V)}/\text{As(III)})$ at pH 3 and pH 9 are 0.40
373 V and -0.2 V, respectively [39]. This will provide the chance for $\cdot\text{O}_2^-$, as a weak
374 oxidant, to directly oxidize As(III) at high pH, when $\cdot\text{OH}$ is in short. It has been
375 reported that superoxide radicals can act as the main free radicals to oxidize arsenic at
376 pH 9 [39,40]. Combining with the results from the quenching experiments (Fig. 6e
377 and 6f), it can be reasonably deduced that $\cdot\text{O}_2^-$ is responsible for the oxidation of
378 As(III) at pH 7 and 11 in our system.



379

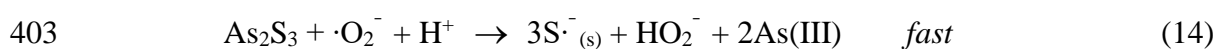
380 **Fig. 7.** (a) sulfur-containing radicals in the sludge by light irradiation for 10 min and
 381 annealing to 90 K. The numbers for peak position are g values. (b) Dissolution of the
 382 sludge (TAs) in sulfite solution under visible light at pH 7. (c) EPR spectrum of sulfite
 383 radical after 10 min reaction by adding 1 mM sulfite in the sludge system.

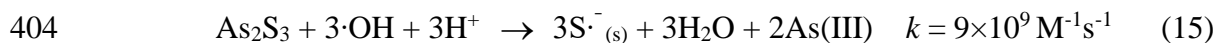
384 **3.9. Photo-generated active sulfur radicals and their effects on the production of**

385 **S₈**

386 Visible light irradiation not only accelerates the release and oxidation of As(III)
387 from ASS, but also promotes the production of sulfur-related ions and the solid phase
388 S₈. In order to understand the transformation of sulfur species and their effects on the
389 dissolution of ASS, active sulfur species that are expected to form under light
390 illumination, were monitored by EPR at 90 K. As shown in Fig. 7a, multiple peaks
391 located at the magnetic field of 3150-3400 G were observed at all three pH values.
392 These were sulfur-containing free radicals, S^{·-}_(s), at g = 2.052~2.021 [41,42] and
393 sulfur-oxide anion radicals, SO₂^{·-}, at g = 2.003 [19]. Normally, sulfide containing
394 radicals are difficult to capture in an aerobic environment, due to readily reacting with
395 oxygen and thus having an extremely short lifetime [19]. Also, the radicals are very
396 sensitive to temperature and the measured spectra gradually diminish on warming.
397 Thus, the measurement has to be done at a low temperature (90 K in our case).

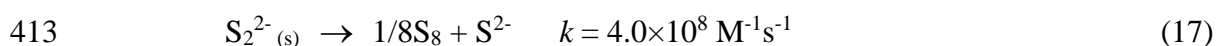
398 It has been reported that under light irradiation, sulfur radicals can be produced
399 from the trapped photo-generated holes localized on the lattice sulfur ions with
400 surface defects or impurities [42]. Therefore, it can be reasonably deduced that in our
401 system, ·O₂⁻ and ·OH can react with the lattice sulfur on the surface of As₂S₃ to form
402 sulfur-containing radicals, as described in eqs 14-15 [19,43].



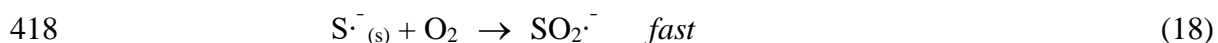


405 During the photo-reaction process, As(III) can be released. The specific species of the
 406 released As(III) is highly dependent on the pH values and S^{2-} concentration. For
 407 example, H_3AsO_3 is the main species in the acid and neutral solution with little S^{2-}
 408 ions, while arsenic sulfide complexes, such as AsS_2^- , HAS_2S_4^- , $\text{H}_2\text{As}_3\text{S}_6^-$ and
 409 $\text{As(OH)}_x(\text{SH})_y^{3-x-y}$, form in the basic solution with a high concentration of S^{2-} [10-12].

410 The generation of sulfide containing radicals, $\text{S}\cdot_{(\text{s})}^-$, will then transform into S_2^{2-}
 411 and finally produce S_8 , as presented in eqs 16 and 17 [44].



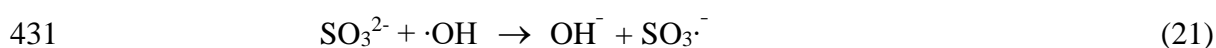
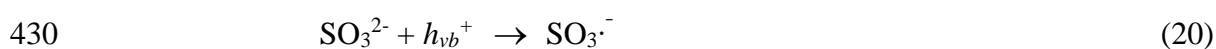
414 Alternatively, $\text{S}\cdot_{(\text{s})}^-$ can react with dissolving oxygen and convert to $\text{SO}_2\cdot^-$, and then
 415 quickly decompose to yield $\cdot\text{O}_2^-$, as described in eqs 18 and 19, which leads to the
 416 weak EPR signals of sulfur radicals detectable even at a very low temperature (Fig. 7a)
 417 [45].



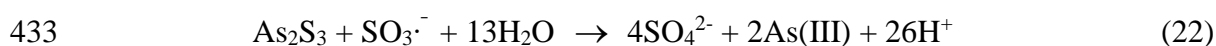
420 **3.10. The effects of intermediate sulfur species on the dissolution of ASS**

421 During the dissolution of ASS under visible light, the intermediate sulfur species,
 422 such as S^{2-} , SO_3^{2-} and $\text{S}_2\text{O}_3^{2-}$, were detected in the system (Fig. 4). In order to
 423 understand the effect of these sulfur species on the dissolution of ASS, extra

424 sulfur-containing salts were employed into the system during illumination. As shown
425 in Fig. 7b, when Na₂SO₃ was added, the dissolution of ASS was accelerated under
426 light irradiation. The EPR result revealed that with the addition of Na₂SO₃ in the
427 sludge, a new and strong signal of SO₃^{·-} [46] was observed under visible light (Fig.
428 7c). The generation of SO₃^{·-} was possibly from either photo-generated holes (eq 20)
429 or hydroxyl radicals (eq 21) [47].

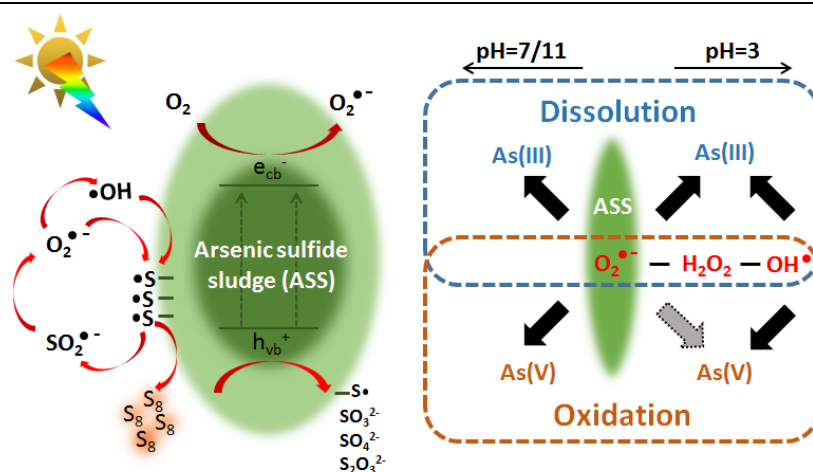


432 The dissolution of ASS can be accelerated by SO₃^{·-}, as follows:



434 However, the addition of extra S²⁻ or S₂O₃²⁻ resulted in a decrease in dissolution
435 rate of ASS (Fig. S8), where S²⁻ and S₂O₃²⁻ may act as the electron donors scavenging
436 active oxygen species that contribute to the dissolution of ASS. Notably, no SO₄^{·-}
437 was found in all the experimental systems mentioned above, which was verified by
438 using methanol as the scavenger.

439



440

441 **Fig. 8.** Conceptual model of the photocatalytic dissolution and oxidation of arsenic
 442 sulfide sludge.

443

444 **4. Conclusion**

445 In the environment, a larger amount of arsenic sludge is discharged and
 446 deposited, especially during the treatment of acid mining and ore smelting wastewater.
 447 The sludge poses a major environmental threat, due to the potential release of arsenic
 448 ions. When the sludge is exposed to solar light irradiation, not only the release rate of
 449 As(III), but also the oxidation rate of As(III) to As(V) can be markedly accelerated,
 450 which will further increase the environmental risk of the discharged sludge. The
 451 mechanism of release and oxidation of As(III) from ASS accelerated by visible light is
 452 proposed as follows (Fig. 8). The ASS produces photo-generated holes (h_{vb}^+) and
 453 electrons (e_{cb}^-) under illumination, which will further react with the species (e.g.
 454 oxygen, hydroxide or sulfur) in solution to produce the corresponding active free
 455 radicals. $\cdot O_2^-$ is the primary free radical in the system, both for forming $OH\cdot$ and

456 sulfur-containing radicals and for releasing and oxidizing As(III) from ASS. At the
457 higher pH (7 or 11), both the dissolution and the oxidation of the sludge are directly
458 accelerated by $\cdot\text{O}_2^-$. At the lower pH (3), the dissolution of the sludge is promoted by
459 both $\cdot\text{O}_2^-$ and $\cdot\text{OH}$, while the oxidation of As(III) is mainly by $\cdot\text{OH}$. In the solid phase,
460 the hydrophobic S_8 is formed on the surface of ASS through a series of sulfur radicals
461 ($\text{S}^{\cdot-}_{(s)}$ and $\text{SO}_2^{\cdot-}$) involved reactions, which favors the agglomeration and precipitation
462 of ASS. In addition, the dissolution of ASS generates the intermediate sulfur species,
463 in which SO_3^{2-} positively contributes to its dissolution by converting into $\text{SO}_3^{\cdot-}$ under
464 visible light.

465 In order to check the dissolution and transformation of ASS in the environment,
466 experiments were conducted under actual sunlight. Similar results were obtained as
467 the simulated experiments, in which both the release of As(III) ions from ASS and the
468 oxidation of As(III) into As(V) were accelerated by actual sunlight (see Fig.S9). The
469 dissolution and oxidation rates of ASS under actual sunlight were much slower than
470 those under simulated light, due to the unstable and weak intensity of actual sunlight.
471 The finding in this work is meaningful to inform the development of an effective
472 strategy for the safe stocking and treatment of slag residue. In addition, the
473 photochemical reactions on the ASS can generate active oxygen and sulfur species
474 under light illumination. These entities will not only affect the migration and
475 transformation behaviors of heavy metals ions and organic compounds in the

476 environment, but also interfere with the geochemical cycle process of the important
477 elements, such as sulfur. Further studies on limiting the dissolution and oxidation of
478 the deposited ASS in natural environments, and/or the development of methods to
479 extract arsenic for detoxifying the sludge and resource recycling, are required to
480 support future improvements in environmental management at relevant industry sites.

481

482 **Acknowledgements**

483 The authors acknowledge the financial support from National Key Research and
484 Development Program of China (2017YFA0207204 and 2016YFA0203101), the
485 National Natural Science Foundation of China (Grant No. 21876190 and 21836002),
486 the Key Research and Development Program of Ningxia (2017BY064), and the “One
487 Hundred Talents Program” in Chinese Academy of Sciences.

488

489 **Appendix A. Supplementary data**

490 Supplementary data of this article include the reagents, the detailed analysis methods
491 of sulfur species, chemical compositions (from XRF and ICP), UV-vis spectra of raw
492 ASS, XPS spectra and photo of ASS with and without visible light irradiation, and the
493 effects of dissolved oxygen, S^{2-} and $S_2O_3^{2-}$ on ASS.

494

495

496 **References**

- 497 [1] W.R. Cullen, K.J. Reimer, *Chem. Rev.* 89 (1989) 713-764.
- 498 [2] P.A. Riveros, J.E. Dutrizac, P. Spencer, *Can. Metall. Quart.* 40 (2001) 395-420.
- 499 [3] H.E. Jamieson, *Rev. Mineral. Geochem.* 79 (2014) 533–587.
- 500 [4] R.P. Liu, Z.C. Yang, Z.L. He, L.Y. Wu, C.Z. Hu, W.Z. Wu, J.H. Qu, *Chem. Eng. J.*
- 501 304 (2016) 986-992.
- 502 [5] L. Kong, X. Peng, X. Hu, *Environ. Sci. Technol.* 51 (2017) 12583-12591.
- 503 [6] A. Lewis, R. Van Hille, *Hydrometallurgy*, 81 (2006) 197-204.
- 504 [7] L. Guo, Y. Du, Q. Yi, D. Li, L. Cao, D. Du, *Sep. Purif. Technol.* 142 (2015)
- 505 209-214.
- 506 [8] A. Bhattacharya, J. Routh, G. Jacks, P. Bhattacharya, M. Morth, *Appl. Geochem.*
- 507 21 (2006) 1760-1780.
- 508 [9] L.E. Eary, *Geochim. Cosmochim. Acta.* 56 (1992) 2267-2280.
- 509 [10] R.M. Floroiu, A.P. Davis, A. Torrents, *Environ. Sci. Technol.* 38 (2004)
- 510 1031-1037.
- 511 [11] S. Stauder, B. Raue, F. Sacher, *Environ. Sci. Technol.* 39 (2005) 5933-5939.
- 512 [12] R.T. Wilkin, D. Wallschlager, R.G. Ford, *Geochem. T.* 4 (2003) 1-7.
- 513 [13] X. Hu, L. Kong, M. He, *Environ. Sci. Technol.* 48 (2014) 14266-14272.
- 514 [14] X.Y. Hu, M.C. He, L.H. Kong, *Appl. Geochem.* 61 (2015) 53-61.
- 515 [15] X.Y. Hu, X.J. Peng, L.H. Kong, *Environ. Sci. Technol.* 52 (2018) 1954-1962.

-
- 516 [16] G. Mills, Z.G. Li, D. Meisel, *J. Phys. Chem.* 92 (1988) 822-828.
- 517 [17] S. Hu, J.S. Lu, C.Y. Jing, *J. Environ. Sci.* 24 (2012) 1341-1346.
- 518 [18] J.D. Cline, *Limnol. Oceanogr.* 14 (1969) 454-458.
- 519 [19] J. Zhu, K. Petit, A.O. Colson, S. Debolt, M.D. Sevilla, *J. Phys. Chem.* 95 (1991)
- 520 3676-3681.
- 521 [20] O. Kondrat, R. Holomb, A. Csik, V. Takats, M. Veres, V. Mitsa, *Nanoscale Res.*
- 522 *Let.* 12 (2017) 149.
- 523 [21] D.S. Han, B. Batchelor, A. Abdel-Wahab, *J. Colloid Interface Sci.* 368 (2012)
- 524 496-504.
- 525 [22] H. Chen, Z.L. Zhang, Z.L. Yang, Q. Yang, B. Li, Z.Y. Bai, *Chem. Eng. J.* 273
- 526 (2015) 481-489.
- 527 [23] A.C. Scheinost, R. Kirsch, D. Banerjee, A. Fernandez-Martinez, H. Zaenker, H.
- 528 Funke, L. Charlet, *J. Contam. Hydrol.* 102 (2008) 228-245.
- 529 [24] W.M. Liu, S. Chen, *Wear* 238 (2000) 120-124.
- 530 [25] M. Sadiq, T.H. Zaidi, A.A. Mian, *Water Air Soil Pollut.* 20 (1983) 369-377.
- 531 [26] X. Peng, J. Chen, L. Kong, X. Hu, *Environ. Sci. Technol.* 52 (2018) 4794-4801.
- 532 [27] M.F. Lengke, R.N. Tempel, *Geochim. Cosmochim. Acta.* 65 (2001) 2241-2255.
- 533 [28] X. Xu, R.J. Lu, X.F. Zhao, Y. Zhu, S.L. Xu, F.Z. Zhang, *Appl. Catal. B Environ.*
- 534 125 (2012) 11-20.

-
- 535 [29] B. Luo, D. Xu, D. Li, G. Wu, M. Wu, W. Shi, M. Chen, ACS Appl. Mat.
536 Interfaces 7 (2015) 17061-17069.
- 537 [30] J.G. Guo, Y. Liu, Y.J. Hao, Y.L. Li, X.J. Wang, R.H. Liu, F.T. Li, Appl. Catal. B
538 Environ. 224 (2018) 841-853.
- 539 [31] J. C. Wang, J. Ren, H.C. Yao, L. Zhang, J.S. Wang, S.Q. Zang, L.F. Han, Z.J. Li,
540 J. Hazard. Mater. 311 (2016) 11-19.
- 541 [32] J. Wang, W.J. Jiang, D. Liu, Z. Wei, Y.F. Zhu, Appl. Catal. B Environ. 176 (2015)
542 306-314.
- 543 [33] J.C. Sin, S.M. Lam, I. Satoshi, K.T. Lee, A.R. Mohamed, Appl. Catal. B Environ.
544 148 (2014) 258-268.
- 545 [34] Z. Zhang, F. Yu, L. Huang, J. Jiatieli, Y. Li, L. Song, N. Yu, D.D. Dionysiou, J.
546 Hazard. Mater. 278 (2014) 152-157.
- 547 [35] X.H. Jiang, Q.J. Xing, X.B. Luo, F. Li, J.P. Zou, S.S. Liu, X. Li, X.K. Wang,
548 Appl. Catal. B Environ. 228 (2018) 29-38.
- 549 [36] P.S. Rao, E. Hayon, J. Phys. Chem. 79 (1975) 397-402.
- 550 [37] M. Sun, G. Zhang, Y. Qin, M. Cao, Y. Liu, J. Li, J. Qu, H. Liu, Environ. Sci.
551 Technol. 49 (2015) 9289-9297.
- 552 [38] B. Jiang, J. Guo, Z. Wang, X. Zheng, J. Zheng, W. Wu, M. Wu, Q. Xue, Chem.
553 Eng. J. 262 (2015) 1144-1151.
- 554 [39] H. Lee, W. Choi, Environ. Sci. Technol. 36 (2002) 3872-3878.

-
- 555 [40] J. Ryu, W. Choi, *Environ. Sci. Technol.* 38 (2004) 2928-2933.
- 556 [41] S. Yanagida, K. Mizumoto, C. Pac, *J. Am. Chem. Soc.* 108 (1986) 647-654.
- 557 [42] K.C. Khulbe, R.S. Mann, *Zeitschrift Fur Physikalische Chemie-Leipzig* 271
558 (1990) 1263-1270.
- 559 [43] R. Wedmann, S. Bertlein, I. Macinkovic, S. Boltz, J. Miljkovic, L.E. Munoz, M.
560 Herrmann, M.R. Filipovic, *Nitric Oxide* 41 (2014) 85-96.
- 561 [44] C.A. Linkous, C.P. Huang, J.R. Fowler, *J. Photochem. Photobiol. A-Chem.* 168
562 (2004) 153-160.
- 563 [45] T.N. Das, R.E. Huie, P. Neta, S. Padmaja, *Journal of Phys. Chem. A* 103 (1999)
564 5221-5226.
- 565 [46] K. Rangelova, A.B. Rice, A. Khajo, M. Triquigneaux, S. Garantziotis, R.S.
566 Magliozzo, R.P. Mason, *Free Radic. Biol. Med.* 52 (2012) 1264-1271.
- 567 [47] J. Zhang, L. Zhu, Z. Shi, Y. Gao, *Chemosphere* 186 (2017) 576-579.